Surface facet dependence of competing alloying mechanisms

Yicheng Wang, Konstantinos G. Papanikolaou, Ryan T. Hannagan, Dipna A. Patel, Tedros A. Balema, Laura A. Cramer, Paul L. Kress, Michail Stamatakis, and E. Charles H. Sykes

COLLECTIONS

Paper published as part of the special topic on Special Collection in Honor of Women in Chemical Physics and Physical ChemistryWCP2020

View Online   **Export Citation**   **CrossMark**

ARTICLES YOU MAY BE INTERESTED IN

Surface facet dependence of competing alloying mechanisms

View Online   Export Citation   CrossMark

Yicheng Wang,[1] [ID] Konstantinos G. Papanikolaou,[2] [ID] Ryan T. Hannagan,[1] Dipna A. Patel,[1] Tedros A. Balema,[1] Laura A. Cramer,[1] Paul L. Kress,[1] Michail Stamatakis,[2,a)] [ID] and E. Charles H. Sykes[1,a)] [ID]

AFFILIATIONS

[1] Department of Chemistry, Tufts University, 62 Talbot Avenue, Medford, Massachusetts 02155, USA

[2] Thomas Young Centre and Department of Chemical Engineering, University College London, Roberts Building, Torrington Place, London WC1E 7JE, United Kingdom

Note: This paper is part of the JCP Special Collection in Honor of Women in Chemical Physics and Physical Chemistry.
a) Authors to whom correspondence should be addressed: m.stamatakis@ucl.ac.uk and charles.sykes@tufts.edu

ABSTRACT

Metal alloys are ubiquitous in many branches of heterogeneous catalysis, and it is now fairly well established that the local atomic structure of an alloy can have a profound influence on its chemical reactivity. While these effects can be difficult to probe in nanoparticle catalysts, model studies using well defined single crystal surfaces alloyed with dopants enable these structure–function correlations to be drawn. The first step in this approach involves understanding the alloying mechanism and the type of ensembles formed. In this study, we examined the atomic structure of RhCu single-atom alloys formed on Cu(111), Cu(100), and Cu(110) surfaces. Our results show a striking difference between Rh atoms alloying in Cu(111) vs the more open Cu(100) and Cu(110) surface facets. Unlike Cu(111) on which Rh atoms preferentially place-exchange with Cu atoms in the local regions above step edges leaving the majority of the Cu surface free of Rh, highly dispersed, homogeneous alloys are formed on the Cu(100) and (110) surfaces. These dramatically different alloying mechanisms are understood by quantifying the energetic barriers for atomic hopping, exchange, swapping, and vacancy filling events for Rh atoms on different Cu surfaces through theoretical calculations. Density functional theory results indicate that the observed differences in the alloying mechanism can be attributed to a faster hopping rate, relatively high atomic exchange barriers, and stronger binding of Rh atoms in the vicinity of step edges on Cu(111) compared to Cu(110) and Cu(100). These model systems will serve as useful platforms for examining structure sensitive chemistry on single-atom alloys.

Published under license by AIP Publishing. https://doi.org/10.1063/5.0034520

I. INTRODUCTION

Single-atom alloys (SAAs) are an emerging class of heterogeneous catalysts in which trace amounts of a reactive metal dopant exist in the form of isolated atoms in a less reactive but more selective host metal.[1–16] The unique electronic and geometric properties of these SAA catalysts give rise to enhanced selectivity and stability for many reactions, deviations from "traditional" transition metal scaling relationships that limit catalyst performance, free-atom like d-states, and resistance to common catalyst poisons.[7,13,17,18] As such, there has been widespread interest in these new materials in both the surface science and heterogeneous catalysis communities. However, the vast majority of the model system research has been conducted on (111) terminated surfaces,

as (111) is the most commonly exposed facet of face-centered cubic (fcc) metal nanoparticles. To date, PtCu(111), PdCu(111), PdAu(111), PtAg(111), NiCu(111), NiAu(111), RhCu(111), and PdAg(111) SAA model catalysts have been reported.[1,19–25] Despite the thorough study of (111) terminated SAA surfaces, little research has been done on more under-coordinated (100) and (110) surfaces.

Structure sensitivity plays an important role in catalysis with the classic example of NH_3 synthesis on body-centered cubic (bcc) Fe(111), Fe(100), and Fe(110), where the more open/undercoordinated Fe(111) surface exhibits the highest dissociative N_2 sticking coefficient and is responsible for the overall activity of the industrial catalyst.[26,27] In terms of hydrocarbon chemistry, Jenks *et al.* examined the behavior of iodomethane

and iodoethane on Cu(111), Cu(100), and Cu(110) by using temperature-programmed desorption (TPD). Their results revealed that methylene coupling and β-hydride elimination are structure sensitive, while α-hydride elimination is not. At high methyl iodide coverage, ethane desorption was 40 K lower for Cu(110) compared to Cu(100) and Cu(111), which represents approximately two orders of magnitude difference in the reaction rates.[28] Specific to SAA catalysts, Gao *et al.* investigated higher alcohol synthesis on RhCu(111) and RhCu(100) SAA surfaces using Density Functional Theory (DFT). The energetic landscapes indicated that methanol formation is favored on RhCu(111), while ethanol may be the preferred product on RhCu(100).[29] Jiang *et al.* experimentally studied the semihydrogenation of phenylacetylene on PdCu SAA nanosheets and nanocubes with predominantly (111) and (100) surfaces exposed, respectively.[30] The authors concluded that while hydrogen spillover from the isolated Pd atoms to Cu occurred on both Cu surface facets, the H atoms that had spilled over were only active for phenylacetylene semi-hydrogenation on Cu(100). The lower barrier for the addition of the first H atom and the stronger phenylacetylene adsorption on Cu(100) vs Cu(111) were proposed as the reasons for the higher observed activity of the PdCu(100) based catalyst. However, such nanoparticle studies cannot completely rule out the contribution from minor exposed facets or adsorbate-induced reconstructions. Examining single crystals under ultrahigh vacuum (UHV), as we do in this paper, enables us to study the structure and alloying mechanism in well-defined facets with atomic-scale imaging resolution.

Theory work by Papanikolaou *et al.* has shown that SAA preparation is thermodynamically feasible on the (100) surface, as isolated dopant atoms have a positive aggregation energy, thereby remaining dispersed as isolated sites rather than agglomerating into dopant clusters.[31] They also reported that the binding of CO is similar to SAAs formed on the (111) and (100) facets of Cu. For instance, the CO binding energies for RhCu(111) and RhCu(100) are −1.71 eV and −1.75 eV, respectively. Therefore, we may expect a similar reactivity on (100) and (111) surfaces, as the adsorption strength of small molecules often scales with reactivity. Modeling of CO_2, N_2, and NO dissociation was conducted to probe the structure sensitivity of SAAs in Cu(100) and Cu(111) using DFT. These reactions exhibit similar structure sensitivity on SAAs and coinage metal surfaces, which is considerably less than platinum group metal (PGM) surfaces. For example, the dissociation barriers for CO_2 on RhCu(100) and RhCu(111) are 0.74 eV and 0.63 eV, respectively. This small degree of structure sensitivity can be attributed to slight differences in the electronic state of the Rh atom, which arise from the different coordination environments of Rh in the two surfaces.[32] However, direct experimental evidence for SAA structure sensitivity on well-defined facets remains very limited. The first step toward elucidating the aforementioned effects involves the construction of SAA model catalysts on more open surfaces, and the key to that is a thorough understanding of alloy mechanisms of dopant atoms on these surface facets.

In this paper, we present a combined scanning tunneling microscopy (STM) and DFT study of the strikingly different alloying mechanisms of Rh in different facets of Cu. We find that Rh forms dense brims on the Cu(111) surface, whereas in the more open (110) and (100) surfaces, Rh alloys uniformly across the terraces. Our calculations reveal that this occurs because of a delicate balance

between diffusion and place-exchange barriers at different surface sites on the different surface facets. Overall, this work highlights the importance of the surface structure of the host material on alloying behavior, and these systems serve as well-defined model catalyst surfaces with which to interrogate the effect of structure sensitivity on SAA reactivity.

II. EXPERIMENTAL METHODS

A. Low-temperature scanning tunneling microscopy (LT-STM)

LT-STM experiments were conducted in UHV with a base pressure of ~1 × 10⁻¹¹ mbar using an Omicron LT-STM. Sample cleaning was performed in the adjacent preparation chamber with the base pressure less than 2 × 10⁻¹⁰ mbar. Repeated cycles of Ar (Airgas 99.99%) ion bombardment and thermal annealing to 750 K were used for cleaning the Cu(111), Cu(100), and Cu(110) single crystals. Rh deposition was performed with a Rh rod (Goodfellow 99.9%) in a flux monitored by using an EFM 3 (Scienta Omicron) electron beam evaporator, while the Cu sample temperature was held at 380 K during deposition of a constant flux of ~0.01 ML min⁻¹. The STM images were acquired after cryogenically cooling the STM stage to 80 K.

B. Computational details

DFT calculations were performed using the Vienna *ab initio* simulation package (VASP).[33,34] The electron–ion interactions were treated by the projector augmented method (PAW),[35] and the wave functions of the valence electrons were expanded by plane waves with a kinetic energy cutoff of 400 eV. To describe the exchange and correlation effects, we employed the Perdew–Burke–Ernzerhof (PBE) functional.[36] Using this functional, we computed a lattice constant for Cu of 3.63 Å, which is in excellent agreement with the previous works and in reasonable agreement with the experimental value of 3.59 Å.[37] The electronic wave function was converged to 10⁻⁷ eV, and the Hellman–Feynman forces were relaxed to less than 10⁻² eV Å⁻¹. The low-index SAA Rh/Cu(111), Rh/Cu(100), Rh/Cu(110), and Rh/Cu(211) surfaces were modeled by a four-layer p(4 × 4), a four-layer p(4 × 4), an eight-layer p(4 × 4), and a four-layer p(4 × 1) cell, respectively (see Fig. S1 in the supplementary material). Some (110) surfaces, such as Au(110) and Pt(110), undergo a transition toward the energetically favored (1 × 2) missing row reconstruction geometry.[38–40] Cu(110), however, is not known to be prone to such a reconstruction, and therefore, our DFT calculations focus on an ideal (1 × 1) geometry.[41] The bottom two layers of the (111), (100), and (211) surfaces were fixed at the PBE-computed Cu lattice constant, while the top two layers and any Rh or Cu adatom thereon were allowed to relax during geometry optimization. For the (110) surface, the bottom four layers were fixed at the Cu lattice constant and the top four ones were allowed to relax. The following Monkhorst–Pack k-point meshes were used to sample the Brillouin zones of the considered surfaces: 4 × 4 × 1 k-point mesh for the (111) surface, 4 × 4 × 1 for the (100) surface, 3 × 4 × 1 for the (110) surface, and 5 × 4 × 1 for the (211) surface.[42] Finally, transition states were identified

with the dimer method,[43] and vibrational analyses were performed in order to verify that each of the located transition states was a first order saddle point in the potential energy surface (PES). The adsorption energy of a Rh atom on a Cu surface and the reported activation barriers were calculated by the following equations:

$$E_{ads}(\text{Rh}) = E_{tot}^{Rh+Slab} - E_{tot}^{Slab} - E_{tot}^{Rh(g)}, \tag{1}$$

$$E_a = E_{TS} - E_{IS}, \tag{2}$$

where $E_{tot}^{Rh+Slab}$, E_{tot}^{Slab}, and $E_{tot}^{Rh(g)}$ are the total DFT energies for a Cu slab with a Rh adatom thereon, for a clean Cu slab, and for a Rh atom in the gas phase, respectively. E_{TS} and E_{IS} are the DFT-computed energies for the transition and initial states, respectively.

III. RESULTS AND DISCUSSIONS

A. Scanning tunneling microscopy

The RhCu alloys were prepared by depositing 0.01 monolayers (MLs) of Rh on Cu(111), Cu(100), and Cu(110) single crystals at a substrate temperature of 380 K. As shown in Fig. 1(a), the isolated Rh atoms appear as depressions in the Cu(111) surface. These Rh atoms are densely packed into the regions above step edges, suggesting a preferred alloying mechanism of Rh diffusion to step edges where place-exchange with Cu atoms in the upper terraces occurs, leading to the formation of an alloy brim above the step edges. This alloying mechanism has been observed for many other alloys formed by depositing dopant metals onto (111) surfaces.[19,23,44] In sharp contrast to the (111) facet, our results on the Cu(110) and (100) facets [Figs. 1(b) and 1(c), respectively] reveal that under identical alloying conditions, unlike the (111) surface, Rh atoms are dispersed homogeneously in the Cu(100) and (110) terraces. Importantly, we did not observe any of the dense alloy brims in the regions above step edges for the RhCu alloys in the more open (100) and (110) surfaces. These results indicate that Rh can form SAAs on all three facets of

Cu, in agreement with the previous DFT studies that have revealed an enthalpic preference of Rh atoms to exist as isolated species in Cu(111) and Cu(100) surfaces.[17,31]

The distribution of Rh atoms in the different Cu surface facets suggests that different alloying mechanisms are at play on Cu(111) vs Cu(100) and (110). Place-exchange at step edges appears to be favored for RhCu(111) vs exchange directly into the terraces for RhCu(100) and RhCu(110). While this agrees with the mechanisms previously discussed in the literature, there has never been a direct comparison of alloying the same element into different surface facets under identical alloying conditions.

B. Theoretical investigations

In order to elucidate the disparate alloying behavior exhibited by RhCu(111) and the other two low-index facets investigated (Fig. 1), we performed periodic DFT calculations. These calculations were aimed at elucidating the mechanism by which Rh is incorporated into the Cu host metal and also the mechanism by which Rh adatoms diffuse over the Cu(111), Cu(100), and Cu(110) surfaces. In terms of the diffusion of Rh adatoms, one may simply assume that this process occurs via site-to-site hops, with the Rh adatom sliding over a corrugated plane. Indeed, this is the simplest and most intuitive diffusion mechanism. However, surface science and theoretical studies have demonstrated that adatom diffusion over single crystals can be far more complex than that, thereby highlighting that other types of diffusion, besides *hopping*, merit consideration.[45–47] For example, using an atom probe, Wrigley and Ehrlich argued that the diffusion of a W adatom across the rows of Ir(110) occurs via a concerted *atomic exchange* mechanism.[48] Under these circumstances, the W adatom, which is initially adsorbed on a hollow site, displaces a neighboring Ir atom from a row of the (110) surface, and the latter becomes the "new adatom." This atomic exchange mechanism has been observed and, often, corroborated as the dominant adatom diffusion mechanism in a number of field-ion microscopy

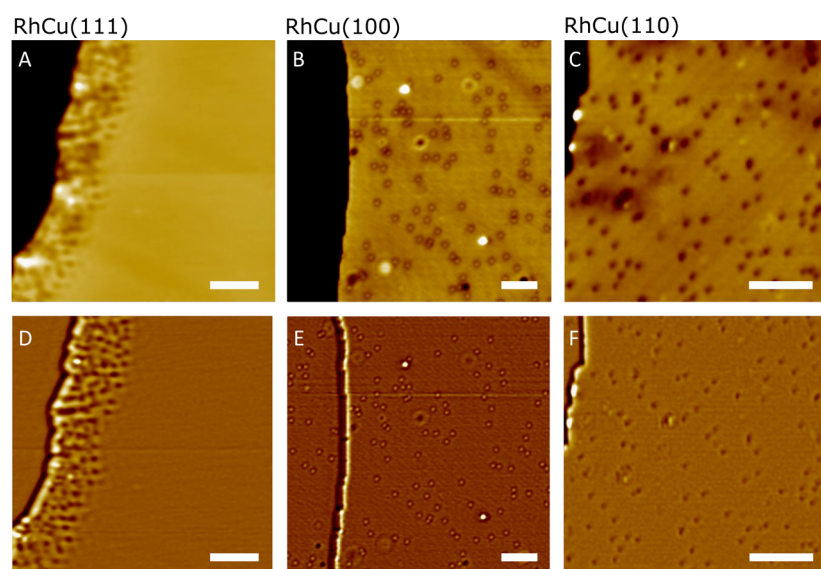RhCu(111)   RhCu(100)   RhCu(110)

FIG. 1. STM images of 0.01 ML RhCu SAAs prepared in the (111), (110), and (100) facets of Cu. (a) RhCu(111) in which dense brims of Rh appear in the regions above step edges and the Rh atoms appear as depressions. (b) RhCu(100) in which isolated Rh atoms can be seen alloyed throughout the terrace with no dense brims at the step edges. (c) RhCu(110) in which isolated Rh atoms are also seen alloyed throughout the terraces. (d)–(f) Derivative STM images corresponding to images (a)–(c) that highlight the Rh alloying sites in different Cu facets. Typical imaging conditions: 300 mV and 300 pA. The scale bars are 5 nm. All SAA surfaces were prepared via Rh deposition on Cu held at 380 K, followed by cooling to 80 K for STM imaging.

and theoretical studies, which focus on low-index facets with an open structure [e.g., (110), (100), and (001)].[49–54] Another possible diffusion mechanism is diffusion via an existing vacancy in the host material. This is the so-called *vacancy-mediated exchange* diffusion,[55] which has been shown to be pronounced on more densely packed surfaces such as Cu(111).[55]

   With this in mind, we used DFT to study the following surface processes on Cu(111), Cu(100), and Cu(110) surface facets: (i) hopping of a Rh adatom from site-to-site on the surface, (ii) atomic exchange between a Rh adatom and a Cu surface atom,

(iii) integration of a Rh adatom into the Cu surface via a vacancy, and (iv) atomic swapping between Rh and Cu surface atoms (Fig. 2). Rh diffusion via hopping involves "jumps" of a Rh adatom from a hollow site to another hollow site via a twofold bridge site, which is the first order saddle point in the PES [Fig. 2(a)]. The hollow sites correspond to fourfold sites on Cu(110) and Cu(100) and threefold sites (either fcc or hcp) on Cu(111) [Fig. 2(a)]. Our results suggest that simple Rh adatom hopping is significantly more facile on the Cu(111) surface ($E_{a,fcc\rightarrow hcp}$ = 0.23 eV or $E_{a,hcp\rightarrow fcc}$ = 0.06 eV) than on Cu(100) ($E_{a,(100)}$ = 0.90 eV) and Cu(110) ($E_{a,(110)}$ = 0.37 eV).
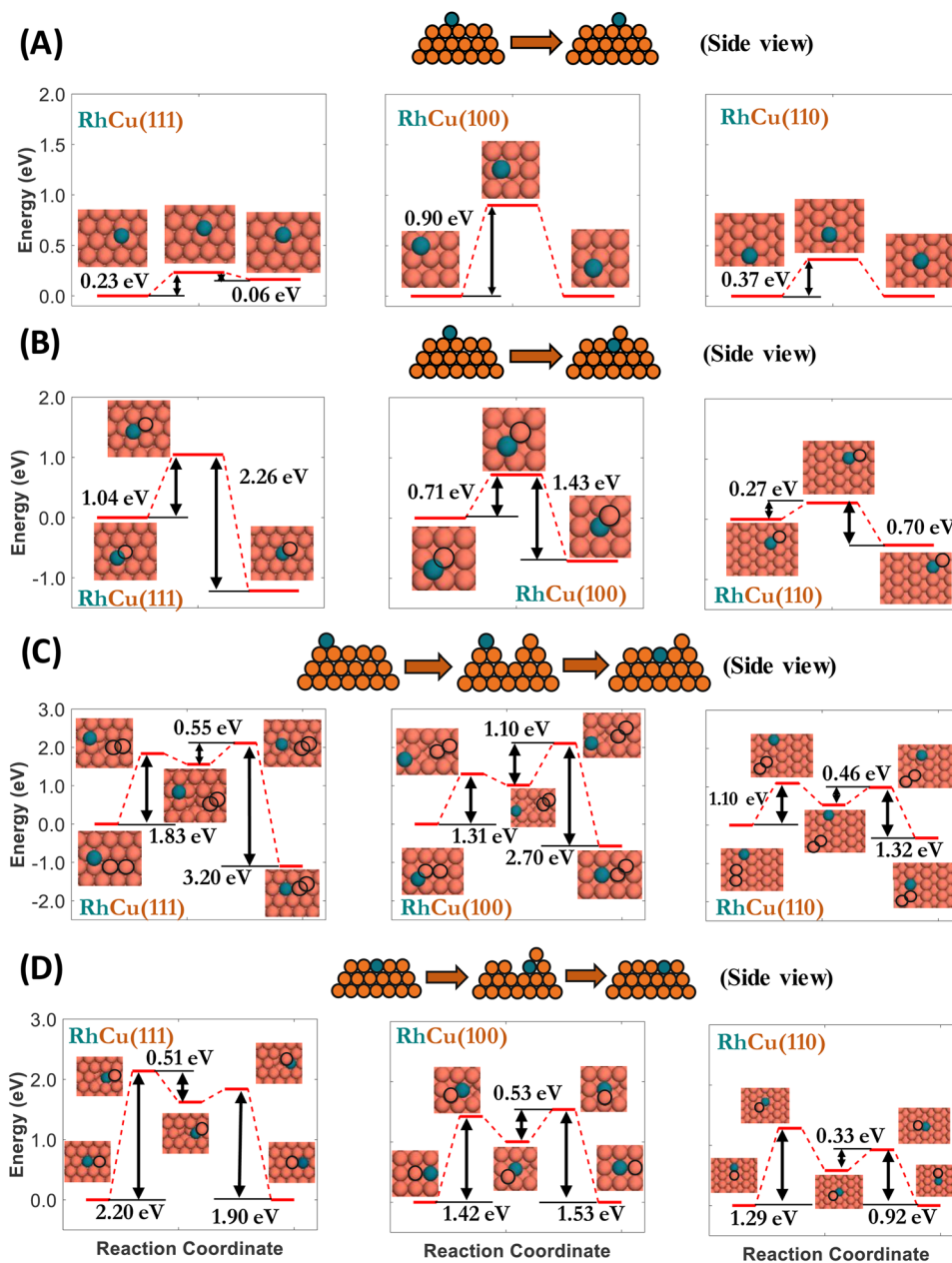

FIG. 2. DFT-computed kinetic barriers for (a) Rh hop diffusion, (b) atomic exchange, (c) Rh integration via a vacancy, and (d) atomic swapping for the three investigated low-index surfaces. A side view representation of the different alloying steps is given above each panel, where we only show states that correspond to a minimum in the PES. Cu and Rh atoms are shown in orange and teal, respectively. Cu atoms that participate in an event are annotated by black circles.

The same trend has been reported for the self-diffusion of Cu over these three low-index surfaces by Hansen *et al.*,[56] and the fast adatom hopping over Cu(111) is in line with the work of Anderson *et al.* on a PbCu(111) system.[55] Importantly, we note that the reported hopping barrier for Cu(110) in Fig. 2(a) involves Rh hopping along the rows of the Cu(110) surface. We have also computed the corresponding barrier for Rh hopping across these rows, and we have found a large kinetic barrier of 1.82 eV (see Fig. S2 of the supplementary material). This high value implies that diffusion across the rows will be highly unlikely via hopping, in qualitative agreement with previous works.[48,54,56]

Atomic diffusion on either pure metal or alloy surfaces often takes place via a concerted mechanism in which more than one atom participates in the diffusion event.[47,57–59] To this end, we continue our investigations by computing the energy barriers for a concerted atomic exchange between a Rh adatom and a Cu atom [Fig. 2(b)]. The atomic exchange proceeds in a similar manner on the three Cu surfaces: the Rh adatom is initially adsorbed on a hollow site; in the transition state, a Cu atom is "lifted-up" by the adatom and a "Rh–Cu dimer" is formed above a surface vacancy; and in the final state, Rh is integrated into the Cu host surface, while the lifted-up Cu atom ends up as an adatom over a mixed hollow site [Fig. 2(b)]. In contrast to the previously discussed hop diffusion [Fig. 2(a)], we find that atomic exchange events are much more easily activated on the open Cu(100) ($E_{a,(100)}$ = 0.71 eV) and Cu(110) ($E_{a,(110)}$ = 0.27 eV) surfaces as compared to Cu(111), where $E_{a,(111)}$ = 1.04 eV. Consequently, the computed barriers in Figs. 2(a) and 2(b) indicate that the predominant alloying mechanism toward the SAA phase will be different among the three low-index surfaces and begins to explain the observed disparate distribution of Rh atoms over these three surfaces (Fig. 1). In particular, our results in Figs. 2(a) and 2(b) demonstrate that Rh atoms that land on Cu(111) will be able to diffuse via hopping across the surface before they experience the appropriate alloying sites (e.g., step edges) that enables them to integrate into the Cu host surface. By contrast, Rh integration via direct atomic exchange into the terraces of the Cu host will be more favorable on Cu(100) and Cu(110) than hopping. This allows Rh adatoms to incorporate easily and directly in the terraces and, therefore, form a uniform and well-dispersed SAA phase over the whole single crystal surface (Fig. 1).

Another mechanism by which Rh can be incorporated into the host material is via an existing vacancy on the Cu host surface [Fig. 2(c)]. To investigate this type of mechanism, we first computed the energy cost for the creation of a vacancy on the Cu crystal [Figs. 2(c) and 3(a)] and then the energy cost for the filling of this vacancy by a Rh adatom. The computed vacancy formation barriers are 1.83 eV for Cu(111), 1.31 eV for Cu(100), and 1.10 eV for Cu(110) [Fig. 2(c)]. According to this result, the more open a surface is, the higher its tendency to form a vacancy. Moreover, we calculated the vacancy formation barrier on the edge of a (211) step [see Fig. 3(b)], which serves as a model of the region around step edges of the Cu crystals seen in Fig. 1. The computed vacancy formation barrier at this site, for a clean Cu(211) surface in the absence of a Rh adatom, is 1.38 eV.

It is noteworthy that the kinetic barrier for vacancy filling [i.e., the second barrier from left to right in the PES of Fig. 2(c)] is 1.10 eV for Cu(100) and 0.46 eV for Cu(110). These values are ~0.40 eV and 0.20 eV larger than the corresponding atomic exchange

barriers, respectively, and merely reflect the difficulty of Rh hop diffusion over these Cu surface facets [Fig. 2(a)]. Consequently, the incorporation of Rh on these surfaces will be more probable via an atomic exchange mechanism even in the presence of vacancies on the host material. In contrast, the vacancy filling barrier on Cu(111) ($E_{a,(111)}$ = 0.55 eV) is almost half of the corresponding atomic exchange barrier [$E_{a,(111)}$ = 1.04 eV]. Therefore, we conjecture that the high concentration of Rh atoms in the vicinity of step edges of Cu(111) (see Fig. 1) may be explained by the following four factors: (i) the fast Rh adatom hopping on Cu(111) [Fig. 2(a)], (ii) the higher susceptibility of the region near the step toward the formation of vacancies as compared to the densely packed (111) plane [Fig. 3(a)], (iii) the relatively easy integration of a Rh adatom into an existing vacancy on the Cu(111) surface [Fig. 2(c)], and (iv) the high stability of a Rh atom embedded in the Cu(111) host surface [see the first inset in Figs. 2(b) and 2(c)].

Furthermore, the significantly stronger binding of Rh in the vicinity of step edges as compared to the threefold sites of Cu(111) [$E(Rh)_{ads,(211)} - E(Rh)_{ads,(111)}$ = −0.96 eV] will be the driving force for Rh migration to the step edges of Cu(111) after deposition [Fig. 3(a)]. This migration is expected to occur through simple and fast hop diffusion. Accordingly, the incorporation of Rh adatoms on Cu(111) will probably occur via the existing or created vacancies, which are more likely to form in the vicinity of the step edges [Fig. 3(a)]. This will lead to a kinetically trapped state, whereby the majority of Rh atoms are incorporated in the region above the step edge (Fig. 1).[19,23–25,44] Depending on the conditions, the system could remain trapped in this metastable state for a considerable amount of time,[55] before reaching equilibrium—namely, a state where entropy will be the driving force toward a well-dispersed SAA phase.[8,17,18,23–25,31,44,60] In contrast, on Cu(100), the atomic exchange events exhibit a relatively small barrier of 0.71 eV, and given the fact that an embedded Rh atom in the Cu host surface exhibits high stability [see Fig. 2(b)], we speculate that the integration of Rh adatoms into the Cu(100) surface will occur at or near their "point of landing," thereby leading to the formation of a uniformly dispersed SAA surface as seen in Fig. 1.

The last type of surface event we studied involves the atomic swapping of an embedded Rh atom and a Cu surface atom [Fig. 2(d)] that leads to the diffusion of the Rh atom in the Cu surface. We find that atomic swapping is not a concerted event (i.e., the initial and final states are not separated by just one transition state) but rather occurs in two steps. The first step involves the displacement of a Cu atom out of the Cu host surface by a neighboring Rh atom; in the second step, the displaced Cu "diffuses back" and fills the created vacancy [Fig. 2(d)]. Our calculations reveal a very large barrier for the first step on RhCu(111) ($E_{a,(111)}$ = 2.20 eV), while the corresponding kinetic barriers for the first step on RhCu(100) and RhCu(110) surfaces are moderate [$E_{a,(100)}$ = 1.42 eV and $E_{a,(110)}$ = 1.29 eV] [Fig. 2(d)]. In this way, atomic swapping and atomic exchange between an embedded Rh atom and a Cu adatom will be equally likely events on RhCu(100), but they will be activated at relatively high temperatures (E_a > 1.40 eV for both events) [see Figs. 2(b) and 2(d)]. In contrast, our results predict that the dominant diffusion event for RhCu(110) will be the atomic exchange [Figs. 2(b) and 2(d)].

Finally, we elucidated the distinctive alloying behavior of the three surfaces further by calculating the approximate rates of the
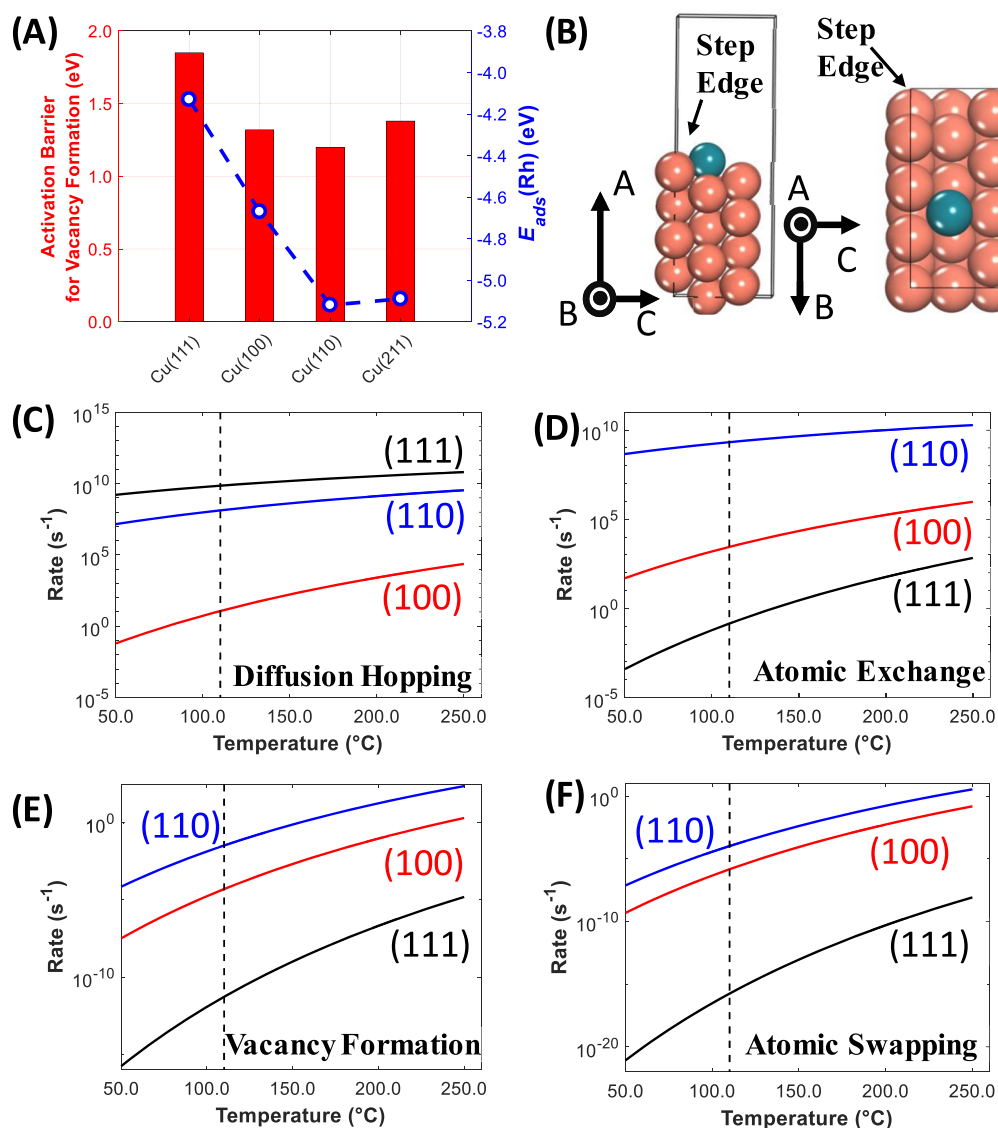
FIG. 3. Energy cost for vacancy formation on pure Cu surfaces and adsorption energies of a Rh adatom on the most stable adsorption site of the same surfaces. The reported barriers in panel (a) refer to clean Cu surfaces in the absence of a Rh adatom. The most stable adsorption site for Rh is a fcc site for Cu(111) and a fourfold site for Cu(100) or Cu(110). (b) The most stable adsorption site for a Rh adatom (teal) on the (211) surface. (c)–(f) Computed rates for Rh hop diffusion, atomic exchange, vacancy formation (in the presence of a Rh adatom in the close vicinity to the vacancy), and atomic swapping, respectively. The dashed line is always at 110 °C, which is the temperature at which alloying was performed in our experiments.

different surface processes. According to the computed kinetic barriers and by using the Eyring equation[61] with a prefactor of $k_B T/h$ (k_B and h are Boltzmann's and Planck's constants, respectively), we computed the approximate rates for the investigated processes within the temperature range of 50 °C – 250 °C [Figs. 3(c)–3(f)]. Since Rh incorporation and atomic swapping are not elementary processes, the reported rates are those for their first steps, which exhibit the largest kinetic barriers. Our principal observation is that atomic exchange, vacancy formation, and atomic swapping are faster on Cu(100) and Cu(110) than on Cu(111) by at least five orders of magnitude at 110 °C [Figs. 3(c)–3(f)], while the opposite holds true for hop based diffusion. This observation further clarifies the disparate behavior of the three facets in relation to the diffusion and incorporation of Rh atoms and suggests that indeed the integration of Rh will occur via different mechanisms on the three surface facets.

IV. CONCLUSIONS

We have examined and directly compared the alloying behavior of small amounts of Rh with Cu(111), Cu(100), and Cu(110) surface facets using STM. In agreement with the previously published results on Cu(111), we observed that most of the Rh atoms are found in dense brims of the isolated sites above step edges. In stark contrast, on the Cu(100) and (110) surfaces, we found that Rh atoms alloy directly into the terrace of Cu(100) and Cu(110) surfaces. This result suggested that the direct exchange of Rh with Cu atoms in terraces is favored on more open surfaces. DFT calculations were used to quantify the relevant energetics behind these striking differences in alloying behavior. We found that the lowest hopping diffusion barrier for Rh atoms occurs on the Cu(111) facet, while atomic exchange is favored over diffusion on Cu(100) and Cu(110) facets. The vacancy filling mechanism was then investigated by examining the activation barrier for vacancy formation and vacancy filling. Vacancy formation on Cu(211) was studied as well to simulate the step edges on Cu(111) where alloying occurs. These results indicated that the vacancy formation barrier is comparable among the Cu(211), Cu(100), and Cu(110) surfaces and much lower than the corresponding barrier on Cu(111). Furthermore, the stronger binding of Rh atoms to Cu sites in the vicinity of step edges acts as a driving force for Rh migration to these sites on Cu(111). Furthermore, the approximate rates for the aforementioned processes were computed in the temperature range of $50\,^{\circ}$C–$250\,^{\circ}$C. The results indicate that atomic exchange, vacancy formation, and atomic swapping occur much faster on Cu(100) and Cu(110), while atomic hopping is much faster on Cu(111). These predictions that Rh atoms tend to become kinetically trapped in the regions above step edges on Cu(111), while atomic exchange and swapping tend to occur on Cu(100) and Cu(110), rationalize our experimental STM results that show a high dispersion of Rh in Cu(100) and (110) vs a preference for the formation of dense alloy regions above step edges on Cu(111). Together, our synergistic experimental–theoretical approach demonstrates and explains the different alloying mechanisms in the three most common facets of Cu and paves the way for a direct cross-comparison of reactivity and the elucidation of structure sensitivity in SAA catalysis.

SUPPLEMENTARY MATERIAL

See the supplementary material for details of the Cu slabs used in the DFT calculations.

AUTHORS' CONTRIBUTIONS

Y.W., K.G.P., M.S., and E.C.H.S. contributed equally to this work.

DEDICATION

This manuscript is dedicated to my former graduate students Professor Ashleigh Baber, Professor Erin Iski, Dr. Heather Tierney, Dr. April Jewell, Dr. Emily Lewis, and Dr. Felicia Lucci. Their hard work and enthusiasm were instrumental in the establishment of the Sykes research group. I owe them a debt of gratitude for their devotion to science and for their continued mentoring of the next generation of scientists.

DATA AVAILABILITY

The data that support the findings of this study are available from the corresponding authors upon reasonable request.

REFERENCES

[1] G. Kyriakou, M. B. Boucher, A. D. Jewell, E. A. Lewis, T. J. Lawton, A. E. Baber, H. L. Tierney, M. Flytzani-Stephanopoulos, and E. C. H. Sykes, Science **335**, 1209 (2012).

[2] F. R. Lucci, J. Liu, M. D. Marcinkowski, M. Yang, L. F. Allard, M. Flytzani-Stephanopoulos, and E. C. H. Sykes, Nat. Commun. **6**, 8550 (2015).

[3] G. Sun, Z. J. Zhao, R. Mu, S. Zha, L. Li, S. Chen, K. Zang, J. Luo, Z. Li, S. C. Purdy, A. J. Kropf, J. T. Miller, L. Zeng, and J. Gong, Nat. Commun. **9**, 4454 (2018).

[4] F. Xing, J. Jeon, T. Toyao, K.-I. Shimizu, and S. Furukawa, Chem. Sci. **10**, 8292 (2019).

[5] M. Luneau, T. Shirman, A. C. Foucher, K. Duanmu, D. M. A. Verbart, P. Sautet, E. A. Stach, J. Aizenberg, R. J. Madix, and C. M. Friend, ACS Catal. **10**, 441 (2020).

[6] H. Li, K. Shin, and G. Henkelman, J. Chem. Phys. **149**, 174705 (2018).

[7] M. T. Darby, R. Réocreux, E. C. H. Sykes, A. Michaelides, and M. Stamatakis, ACS Catal. **8**, 5038 (2018).

[8] K. K. Rao, Q. K. Do, K. Pham, D. Maiti, and L. C. Grabow, Top. Catal. **63**, 728 (2020).

[9] J. Liu, F. R. Lucci, M. Yang, S. Lee, M. D. Marcinkowski, A. J. Therrien, C. T. Williams, E. C. H. Sykes, and M. Flytzani-Stephanopoulos, J. Am. Chem. Soc. **138**, 6396 (2016).

[10] M. B. Boucher, B. Zugic, G. Cladaras, J. Kammert, M. D. Marcinkowski, T. J. Lawton, E. C. H. Sykes, and M. Flytzani-Stephanopoulos, Phys. Chem. Chem. Phys. **15**, 12187 (2013).

[11] M. D. Marcinkowski, M. T. Darby, J. Liu, J. M. Wimble, F. R. Lucci, S. Lee, A. Michaelides, M. Flytzani-Stephanopoulos, M. Stamatakis, and E. C. H. Sykes, Nat. Chem. **10**, 325 (2018).

[12] M. D. Marcinkowski, A. D. Jewell, M. Stamatakis, M. B. Boucher, E. A. Lewis, C. J. Murphy, G. Kyriakou, and E. C. H. Sykes, Nat. Mater. **12**, 523 (2013).

[13] M. T. Greiner, T. E. Jones, S. Beeg, L. Zwiener, M. Scherzer, F. Girgsdies, S. Piccinin, M. Armbrüster, A. Knop-Gericke, and R. Schlögl, Nat. Chem. **10**, 1008 (2018).

[14] B. Seemala, C. M. Cai, C. E. Wyman, and P. Christopher, ACS Catal. **7**, 4070 (2017).

[15] L. Zhou, J. M. P. Martirez, J. Finzel, C. Zhang, D. F. Swearer, S. Tian, H. Robatjazi, M. Lou, L. Dong, L. Henderson, P. Christopher, E. A. Carter, P. Nordlander, and N. J. Halas, Nat. Energy **5**, 61 (2020).

[16] G. X. Pei, X. Y. Liu, X. Yang, L. Zhang, A. Wang, L. Li, H. Wang, X. Wang, and T. Zhang, ACS Catal. **7**, 1491 (2017).

[17] M. T. Darby, E. C. H. Sykes, A. Michaelides, and M. Stamatakis, Top. Catal. **61**, 428 (2018).

[18] R. T. Hannagan, G. Giannakakis, M. Flytzani-Stephanopoulos, and E. C. H. Sykes, Chem. Rev. **120**, 12044 (2020).

[19] F. R. Lucci, T. J. Lawton, A. Pronschinske, and E. C. H. Sykes, J. Phys. Chem. C **118**, 3015 (2014).

[20] J. Liu, M. B. Uhlman, M. M. Montemore, A. Trimpalis, G. Giannakakis, J. Shan, S. Cao, R. T. Hannagan, E. C. H. Sykes, and M. Flytzani-Stephanopoulos, ACS Catal. **9**, 8757 (2019).

[21] Z.-T. Wang, M. T. Darby, A. J. Therrien, M. El-Soda, A. Michaelides, M. Stamatakis, and E. C. H. Sykes, J. Phys. Chem. C **120**, 13574 (2016).

[22] M. Muir and M. Trenary, J. Phys. Chem. C **124**, 14722 (2020).

[23] D. A. Patel, P. L. Kress, L. A. Cramer, A. M. Larson, and E. C. H. Sykes, J. Chem. Phys. **151**, 164705 (2019).

[24] D. A. Patel, R. T. Hannagan, P. L. Kress, A. C. Schilling, V. Çınar, and E. C. H. Sykes, J. Phys. Chem. C **123**, 28142 (2019).

[25] R. T. Hannagan, D. A. Patel, L. A. Cramer, A. C. Schilling, P. T. P. Ryan, A. M. Larson, V. Çınar, Y. Wang, T. A. Balema, and E. C. H. Sykes, ChemCatChem **12**, 488 (2019).

[26] F. Bozso, G. Ertl, and M. Weiss, J. Catal. **50**, 519 (1977).

[27] G. Ertl, Angew. Chem., Int. Ed. **47**, 3524 (2008).

[28] C. J. Jenks, B. E. Bent, N. Bernstein, and F. Zaera, J. Phys. Chem. B **104**, 3008 (2002).

[29] Y. Gao, L. Shi, S. Li, and Q. Ren, Phys. Chem. Chem. Phys. **22**, 5070 (2020).

[30] L. Jiang, K. Liu, S. Hung, L. Zhou, R. Qin, Q. Zhang, P. Liu, L. Gu, H. M. Chen, G. Fu, and N. Zheng, Nat. Nanotechnol. **15**, 848 (2020).

[31] K. G. Papanikolaou, M. T. Darby, and M. Stamatakis, J. Phys. Chem. C **123**, 9128 (2019).

[32] K. G. Papanikolaou and M. Stamatakis, Catal. Sci. Technol. **10**, 5815 (2020).

[33] G. Kresse and J. Hafner, Phys. Rev. B **47**, 558 (1993).

[34] G. Kresse and J. Furthmüller, Comput. Mater. Sci. **6**, 15 (1996).

[35] P. E. Blöchl, Phys. Rev. B **50**, 17953 (1994).

[36] J. P. Perdew, K. Burke, and M. Ernzerhof, Phys. Rev. Lett. **77**, 3865 (1996).

[37] P. Haas, F. Tran, and P. Blaha, Phys. Rev. B **79**, 085104 (2009).

[38] K.-M. Ho and K. P. Bohnen, Phys. Rev. Lett. **59**, 1833 (1987).

[39] E. C. Sowa, M. A. Van Hove, and D. L. Adams, Surf. Sci. **199**, 174 (1988).

[40] I. Matrane, M. Mazroui, R. Ferrando, M. Badawi, and S. Lebègue, Surf. Sci. **690**, 121463 (2019).

[41] J.-M. Zhang, H.-Y. Li, and K.-W. Xu, Surf. Interface Anal. **39**, 660 (2007).

[42] J. D. Pack and H. J. Monkhorst, Phys. Rev. B **16**, 1748 (1977).

[43] G. Henkelman and H. Jónsson, J. Chem. Phys. **111**, 7010 (1999).

[44] M. T. Darby, M. Stamatakis, A. Michaelides, and E. C. H. Sykes, "Lonely atoms with special gifts: Breaking linear scaling relationships in heterogeneous catalysis with single-atom alloys," J. Phys. Chem. Lett. **9**, 5636–5646 (2018).

[45] F. Montalenti and R. Ferrando, Phys. Rev. B **59**, 5881 (1999).

[46] H. Jónsson, Annu. Rev. Phys. Chem. **51**, 623 (2000).

[47] M. Villarba and H. Jónsson, Phys. Rev. B **49**, 2208 (1994).

[48] J. D. Wrigley and G. Ehrlich, Phys. Rev. Lett. **44**, 661 (1980).

[49] B. D. Yu and M. Scheffler, Phys. Rev. B **56**, R15569 (1997).

[50] P. J. Feibelman and R. Stumpf, Phys. Rev. B **59**, 5892 (1999).

[51] R. T. Tung and W. R. Graham, Surf. Sci. **97**, 73 (1980).

[52] P. Wynblatt and N. A. Gjostein, Surf. Sci. **12**, 109 (1968).

[53] P. J. Feibelman, Phys. Rev. Lett. **65**, 729 (1990).

[54] D. W. Bassett and P. R. Webber, Surf. Sci. **70**, 520 (1978).

[55] M. L. Anderson, M. J. D'Amato, P. J. Feibelman, and B. S. Swartzentruber, Phys. Rev. Lett. **90**, 126102 (2003).

[56] L. Hansen, P. Stoltze, K. W. Jacobsen, and J. K. Nørskov, Phys. Rev. B **44**, 6523 (1991).

[57] H. Y. Kim and G. Henkelman, ACS Catal. **3**, 2541 (2013).

[58] B. P. Uberuaga, G. Henkelman, H. Jónsson, S. T. Dunham, W. Windl, and R. Stumpf, Phys. Status Solidi B **233**, 24 (2002).

[59] H. Wang, M. Stamatakis, D. A. Hansgen, S. Caratzoulas, and D. G. Vlachos, J. Chem. Phys. **133**, 224503 (2010).

[60] K. G. Papanikolaou, M. T. Darby, and M. Stamatakis, ACS Catal. **10**, 1224 (2020).

[61] H. Eyring, J. Chem. Phys. **3**, 107 (1935).